NJC

Accepted Manuscript

This article can be cited before page numbers have been issued, to do this please use: S. Chand, M. Mondal, S. C. Pal, A. Pal, S. Maji, D. Mandal and M. C. Das, *New J. Chem.*, 2018, DOI: 10.1039/C8NJ02338G.

ROYAL SOCIETY OF CHEMISTRY

rsc.li/njc

View Article Online
DOI: 10.1039/C8NJ02338G

Revised manuscript
(NJ-ART-05-2018-002338)

Two Azo-functionalized Luminescent 3D Cd(II)-MOFs for Highly Selective Detection of Fe^{3+} and Al^{3+}

Santanu Chand,[a] Manas Mandal,[a] Shyam Chand Pal,[a] Arun Pal,[a] Sinchan Maji,[b] Debaprasad Mandal[b] and Madhab C. Das[a]*

[a]*Department of Chemistry, Indian Institute of Technology Kharagpur, WB, 721302, India*
[b]*Department of Chemistry, Indian Institute of Technology Ropar, Punjab, 140001, India*
E-mail: mcdas@chem.iitkgp.ac.in

Abstract: Two cadmium based 3D luminescent MOFs $\{[Cd_2(SA)_2(L)_2]\cdot H_2O\}_n$ (**Cd-MOF-1**) and $[Cd(CDC)(L)]_n$ (**Cd-MOF-2**) (H_2SA = succinic acid, H_2CDC = 1,4-Cyclohexanedicarboxylic acid, **L** = [3,3'-azobis(pyridine)], S = Guest molecules) have been assembled by employing organic dicarboxylic acid linkers with an unexploited azo functionalized N,N' spacer via room temperature slow evaporation process and characterized by single crystal x-ray analysis, TGA, FT-IR, PXRD and elemental analysis. The topological analysis reveals that **Cd-MOF-1** features a 6c-uninodal rare '***rob***' topology with the point symbol $\{4^8.6^6.8\}$ while **Cd-MOF-2** shows a '***pcu***' alpha-Po primitive cubic topology with the point symbol $\{4^{12}.6^3\}$. These MOFs are highly emissive at 382 nm and 398 nm while excited at 305 nm and 312 nm respectively. The exposed azo groups are presumed to act as functional sites for the recognition of metal ions through quenching of fluorescence intensity. The fluorescence measurements show that these MOFs can selectively and sensitively detect Fe^{3+} as well as Al^{3+} and thus demonstrating the potential for dual-responsive luminescent probe for metal ion sensing. EDS elemental mapping, PXRD of loaded MOF materials, and plausible quenching mechanism have been discussed. More importantly, both the MOFs exhibit rapid response time toward sensing of Fe^{3+} and Al^{3+} as well.

View Article Online
DOI: 10.1039/C8NJ02338G

Introduction

Fe^{3+} is one of the most important and essential element in the human body and biological tissues.[1] However, both excess and deficiency from the normal permissible limit can induce serious disorders.[2] On the other hand, Al is the third most widespread element and the most abundant metal in the biosphere.[3] Excess Al is acquired by the use of deodorants, cookware, cans, antacids and drinking water supplies. Al is not as toxic as heavy metals, but there is evidence of some toxicity if it is consumed in excess.[4] Hence, in virtue of the crucial role of metal ions in the environmental and biological system, the design and synthesis of metal ion sensing probes have attracted much attention of the researchers. Thus it is very important to develop novel candidate as well as novel method that can be easy to apply and ability to detect exclusively Fe^{3+} and Al^{3+} as well.

Microporous luminescent metal-organic frameworks (MOFs) are of interest for their diverse functions, predominantly for the sensing of various metal ions and nitroaromatics.[5-10] Various ways to detect the metal ions have been introduced *via* diverse detection techniques such as inductively coupled plasma atomic emission, atomic absorption spectroscopies etc. Among the various detection methods, fluorometric methods have acquired appreciable attention because of their facilitated detection with rapid response time and easy manipulation with high sensitivity.[7–8] Particularly, the high porosities of MOFs prompt the preconcentration of the analytes (metal ions) in their pores, therefore leading to lower detection limits and higher sensing sensitivities.[9] In recent years, the research on MOF fluorescent chemosensor highlighted the significance of the role of Lewis basic sites within the porous MOFs, such as unsaturated (open) pyridyl group, free $-NH_2$ group, an anionic sulfonate group, and −OH group to enhance unique recognition towards sensing of various metal ions in various solvents.[9-10] For the construction of such kind of MOF materials, researchers are mostly using lanthanides salts due to their sharp and intense luminescence intensity. But, because of the high cost and exiguousness of lanthanides, the MOF sensors based on transition metals are highly desirable.[11] In order to harvest plausible binding sites of selective metal ion sensing, we are interested to immobilize azo functionality of an unexploited spacer 3,3'-azobis(pyridine) with uncoordinated N-rich sites on the MOF backbone. Besides, this spacer possesses a highly conjugated π-electronic system to provide powerful luminescence property. Although a few discrete complexes and hydrogen bonding networks are reported,[12a-b] to the best of our knowledge this spacer has rarely been used for

View Article Online
DOI: 10.1039/C8NJ02338G

the construction of MOF materials.[12c-d] Based on the above considerations, we have designed and constructed two new bifunctional 3D Cd(II)-MOFs ($\{[Cd_2(SA)_2(L)_2]\cdot H_2O\}_n$ (**Cd-MOF-1**) and $\{[Cd(CDC)(L)]\}_n$ (**Cd-MOF-2**)) self-assembled by two different dicarboxylate organic linkers and 3,3'-azobis(pyridine) spacer with exposed azo binding sites for selective sensing of Fe^{3+} as well as Al^{3+} in DMF/water solution. Further investigation on sensing mechanism, detection selectivity in presence of other metal ions and response time have been carried out.

Experimental Section

Materials and reagents.

All the chemicals were of reagent grade quality, and they were purchased from the commercial sources and used as received. The spacer **L** was prepared following a method described in the literature.[12c]

Synthesis of $\{[Cd_2(SA)_2(L)_2]\cdot H_2O\}_n$, Cd-MOF-1. $Cd(NO_3)_2\cdot 4H_2O$ (0.1 mmol, 0.031 g), H_2SA (0.1 mmol, 0.012 g) and L (0.05 mmol, 0.010 g) were dissolved in 3 mL DMF in a glass vial. The resulting solution was stirred at room temperature for 1-2 h, filtered and the filtrate was kept for crystallization at ambient temperature. Block-shaped orange crystals were obtained after about 15-18 days. Yield: 59%. Elemental analysis for C_{28} H_{24} Cd_2 N_8 O_8, calcd: C, 39.87%; H, 3.10%; N, 13.28%. Found: C, 39.84%; H, 3.11%; N, 13.25%. FT-IR (KBr pellet, cm^{-1}): 1659.5(s), 1616.2(w), 1571.7(s), 1495.1(s), 1407.1(s), 1318.4(m), 1288.3(s), 1211.9(s), 1164.5(s), 1133.8(s), 1106.8(s), 870.1(s), 821.2(m), 790.4(s), 748.2(s), 731.6(s), 659.3(s), 624.4(s), 507.1(s), 456.6(s).

Synthesis of $\{[Cd(CDC)(L)]\}_n$, Cd-MOF-2. It has been prepared as described for the synthesis of **1**, except that H_2SA is replaced by H_2CDC (0.1 mmol, 0.017 g). Needle shaped orange crystals were obtained after about 25 days. Yield: 71%. Elemental analysis for C_{18} H_{18} Cd N_4 O_4, calcd: C, 46.31%; H, 3.88%; N, 12.00%. Found: C, 46.28%; H, 4.13.85%; N, 12.09%. FT-IR (KBr pellet, cm^{-1}): 2872.9(w), 1654.5(s), 1607.2(w), 1569.7(s), 1485.1(s), 1387(s), 1318.4(m), 1288.3(s), 1060.2(s), 1013.8(s), 947.3(w), 870.1(s), 821.2(m), 790.4(s), 748.2(s), 731.6(s).

Results and Discussion

The single-crystal X-ray determination reveals 3D coordination frameworks constituted by SA^{2-} or CDC^{2-} and an N,N'-donor spacer **L**. **Cd-MOF-1** crystallizes in

View Article Online
DOI: 10.1039/C8NJ02338G

monoclinic crystal system with $P2_1/n$ space group formulated as $\{[Cd_2(SA)_2(L)_2]\cdot H_2O\}_n$. The asymmetric unit of **Cd-MOF-1** consists of two Cd(II) metal ion, two deprotonated succinic acids and two **L** spacer (Fig. S1, ESI). Each Cd(II) atom is seven-coordinated with two Nitrogen atoms ligated from two different **L** spacer in axial position and five oxygen atoms from three SA^{2-} and thus giving rise a distorted pentagonal bipyramidal configuration $\{CdO_5N_2\}$ (Fig. 1a). The Cd–O bond distances range from 2.330(4) to 2.519(4) Å whereas the Cd–N bond distances range from 2.350(5) to 2.369(5) Å (selected bond distances and angles of **Cd-MOF-1** are listed in Table S2, ESI). Two different coordination modes have been adopted by two carboxylate groups of SA^{2-} ligands, one is bidentate chelating mode and the other is monodentate chelating fashion. Two Cd(II) centers are bridged by two carboxylate groups of SA^{2-} ligands to generate a dimeric $Cd_2(COO)_2$ core unit (Fig. S2, ESI) resulting in the formation of a 1D chain structure along the

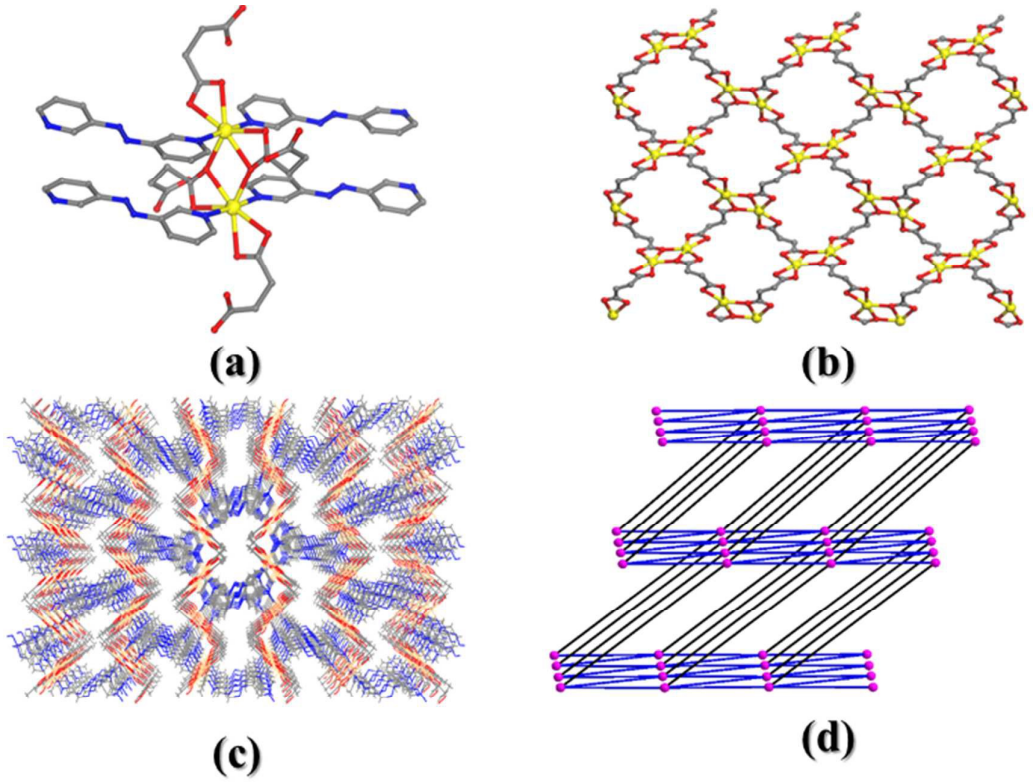

Fig. 1 (a) Coordination environment around Cd(II) in **Cd-MOF-1**. Color code: Cd, yellow; N, blue; O, red; C, grey; H atoms are omitted for clarity. (b) Five coordinated SA^{2-} units with Cd(II) unit to form a 2D layered network. (c) A representation of overall 3D structure along crystallographic '*a*' axis. (d) The topological representation of **Cd-MOF-1** showing overall framework with the rare '***rob***' topology. The pink dots, blue and black sticks represent the $Cd_2(COO)_2$ SBUs, SA^{2-} units and **L** spacers respectively.

View Article Online
DOI: 10.1039/C8NJ02338G

crystallographic 'c' axis (Fig. 1b). The distance between two Cd(II) in the dimeric unit is 3.792 (2) Å. The pyridyl N atoms of the spacer **L** connect the $Cd_2(COO)_2$ unit in a crisscross fashion and extended in both the directions to build an overall 3D network (Fig. 1c). The resultant 3D framework contains the solvent molecules capped in the 1D channel oriented through '*a*' axis (Fig. 1c). Moreover, the framework of **Cd-MOF-1** can be simplified to a 3D uninodal, 6-connected a rare '***rob***' topology with the point symbol $\{4^8.6^6.8\}$ as depicted in Fig. 1d. Weak π····π stacking interaction (centroid to centroid distance of 3.564(2) Å) among the adjacent pyridine moieties of spacer **L** and several non-covalent intermolecular interactions among the ligands further stabilized the framework (Table S3, ESI).

On the other hand, the asymmetric unit of **Cd-MOF-2** consists of one Cd(II) metal ion, one spacer **L**, and one deprotonated CDC^{2-} forming the neutral network with molecular formula **{[Cd(CDC)(L)]}*n*** as depicted in Fig. S3 (ESI). Cd(II) ion is coordinated by four oxygen atoms from three different CDC^{2-} linkers and two nitrogen atoms from two different **L** spacers, showing a distorted octahedral geometry $\{CdO_4N_2\}$ (Fig. 2a). The Cd–O bond distances range from 2.2664(15) to 2.4560(14) Å whereas the Cd–N bond distance ranges from 2.3143(16) to 2.3193(15) Å (selected bond distances and angles of **Cd-MOF-2** are listed in Table S4, ESI). Each CDC^{2-} connects three Cd(II) metal ions through chelating and bridging bidentate fashion forming $Cd_2(CO_2)_2$ (Fig. S4, ESI) units with a separation distance of 3.952(5) Å. Again, these binuclear units are connected with CDC^{2-} ligands forming two dimensional (2D) $[Cd_2(CDC)_2]_n$ sheets lying in the crystallographic '*bc*' plane (Fig. 2b) which are further connected by the spacer **L** to construct a 3D pillared layer dense framework (Fig. 2c). The framework of **Cd-MOF-2** can be simplified to a 3D uninodal, non-interpenetrating '***pcu***' alpha-Po primitive cubic topology network with the point symbol of $\{4^{12}.6^3\}$ (Fig. 2d). Weak π····π stacking interaction (centroid to centroid distance of 3.638(2) Å) among the adjacent pyridyl moieties of spacer **L** and several non-covalent intermolecular interactions among the ligands further stabilized the framework (Table S5, ESI).

To investigate the purity of the crystals in bulk phase PXRD experiment was carried out for both the samples. The as-synthesized and the simulated patterns of PXRD are in good agreement with each other as depicted in Fig. S5 and S6, ESI. To recheck the phase purity in DMF-H_2O mixture (solvent system for sensing measurement studies) we have collected the PXRD upon immerging both **Cd-MOF-1** and **Cd-MOF-2** in 4:1 DMF-H_2O mixture for 12

View Article Online
DOI: 10.1039/C8NJ02338G

hours, which shows the identical peak positions with the as-synthesized sample (Fig. S5 and S6, ESI). To study the thermal behavior, thermogravimetric analysis (TGA) has been carried out from 30 °C to 800 °C in the nitrogen atmosphere with a heating rate 5 °C per min as depicted in Fig. S7-S8 (ESI). TGA of as-synthesized **Cd-MOF-1** shows that a weight loss of 2.2% (calculated 2.1%) occurs below 100 °C which can be attributed to the loss of one lattice water molecule. The framework is stable until 270 °C and after that, the decomposition started gradually. TGA on the as-synthesized **Cd-MOF-2** indicates that the material is stable and no weight loss is observed until 300 °C. The expulsion of the organic ligand and spacer occurs from 350 °C and further heating up to 800 °C reveals continuous weight losses.

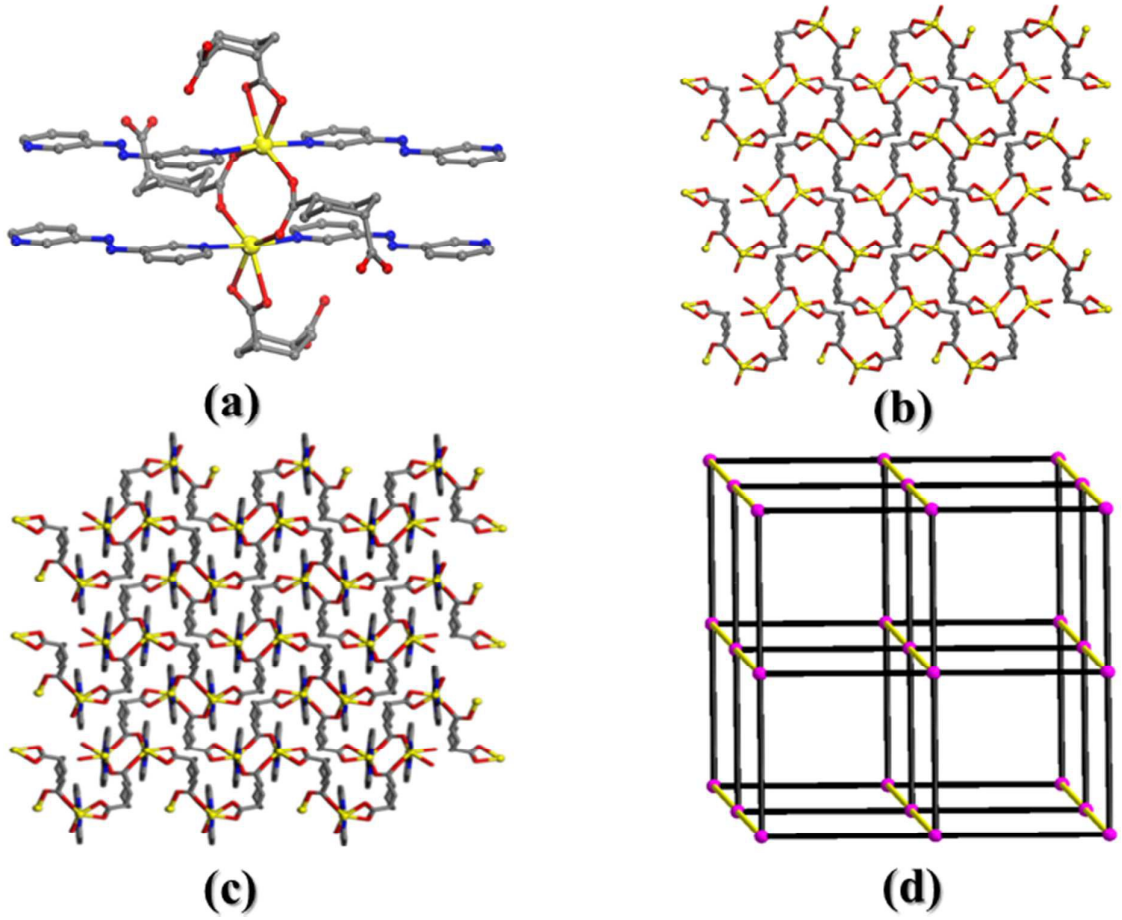

Fig. 2 (a) Coordination environment around Cd(II) in **Cd-MOF-2**. (b) Four coordinated CDC^{2-} units with Cd(II) unit to form a 2D network. (c) A representation of overall 3D structure along crystallographic '*a*' axis. (d) The topological representation of **Cd-MOF-2** showing overall framework with the '***pcu***' alpha-Po primitive cubic topology. The pink dots, black and yellow sticks represent the $Cd_2(COO)_2$ SBUs, CDC^{2-} units and **L** spacers respectively.

View Article Online
DOI: 10.1039/C8NJ02338G

The emission spectra of both **Cd-MOF-1**, as well as **Cd-MOF-2** and the corresponding spacer L, have been investigated in solid state at room temperature as depicted in Fig. S11, ESI. When **Cd-MOF-1** is excited in 305 nm it displays an emission peak at 382 nm that can be attributed to $\pi^* \rightarrow \pi$ and $\pi^* \rightarrow$ n transitions of the spacer (i.e. intra ligand charge transfer transition as well as the ligand to ligand charge transfer transition (LLCT)).[13] On the other hand when **Cd-MOF-2** is excited in 312 nm it displays an emission peak at 398 nm that can be attributed to $\pi^* \rightarrow \pi$ and $\pi^* \rightarrow$ n transitions of the conjugated ligands.

Considering this emission property and presence of uncoordinated Lewis basic azo sites for both the MOFs, we have investigated the fluorescence sensing property towards metal ions. As previously mentioned, the framework has retained its crystallinity in the DMF and water (4:1 mL) mixture of solvents used in this sensing experiment. The standard solution of both the materials have been prepared by adding a finely ground sample of **Cd-MOF-1** and **Cd-MOF-2** (30 mg) in 30 mL DMF solutions and treated by the ultra-sonication for about half an hour. The metal salts (M^{n+} = Na^+, K^+, Ca^{2+}, Mg^{2+}, Ba^{2+}, Fe^{2+}, Ni^{2+}, Cu^{2+}, Cr^{2+}, Hg^{2+}, Cd^{2+}, Pb^{2+}, Al^{3+}, Cr^{3+}, Fe^{3+}) have been prepared in 1 x 10^{-2} (M) solution in water. For all the experiments the excitation wavelength was 305 nm (λ_{ex} = 305 nm). The metal ion detection experiments on both the samples were performed by adding a total 100 µL aqueous solutions with the sequential addition of 5 µL of the different metal ions to a 2 mL of **Cd-MOF-1** or **Cd-MOF-2** in DMF and subsequently measuring the luminescence spectra respectively.

After the addition of metal ion (Fig. 3 and 4) the luminescence spectra of **Cd-MOF-1** display that most metal ions, such as Na^+, K^+, Ba^{2+}, Mg^{2+}, Ca^{2+}, Co^{2+}, Cd^{2+}, Pb^{2+}, Hg^{2+}, and Cu^{2+} make negligible difference to the luminescence intensity (Fig. S12, ESI). On the contrary, Fe^{2+}, Al^{3+}, Cr^{3+} and Fe^{3+} ions display different levels of luminescence quenching. Among the four metal ions, Fe^{3+} and Al^{3+} ions lead to almost complete quenching of intensity of **Cd-MOF-1** indicating its highly selective sensitivity towards both the metal ions. As can be seen, the emission intensity of **Cd-MOF-1** decreases with gradually increasing the concentration of Fe^{3+} and Al^{3+} (5 µL to 100 µL). Quantitatively, the quenching efficiency effect can be explained by using the Stern-Volmer equation: $I_0/I = 1 + K_{sv}[M]$, where I_0 and I are the luminescence intensity of **Cd-MOF-1** before the addition of the metal ion and after the addition of the metal ion respectively, K_{sv} is quenching coefficient and [M] is the molar

View Article Online
DOI: 10.1039/C8NJ02338G

concentration of the metal ion. Hence, it is expected that the decrease in the luminescence intensity will be proportionate to the metal ions concentration. As shown in Fig. S13 (ESI), it is clear that the Stern−Volmer curves for Fe(III) ion are nearly linear at low concentrations. However, with increasing the concentrations, the curves deviate from the linearity which can be explained by an energy-transfer process or self-absorption.[14] Estimated from the plot of fluorescence intensity and the concentration of the metal ions, the experimental result shows the value of K_{sv} = 2.1 ×10^4 M^{-1}, and 5.4 ×10^3 M^{-1} for Fe^{3+} and Al^{3+} respectively, which is comparable and higher than some

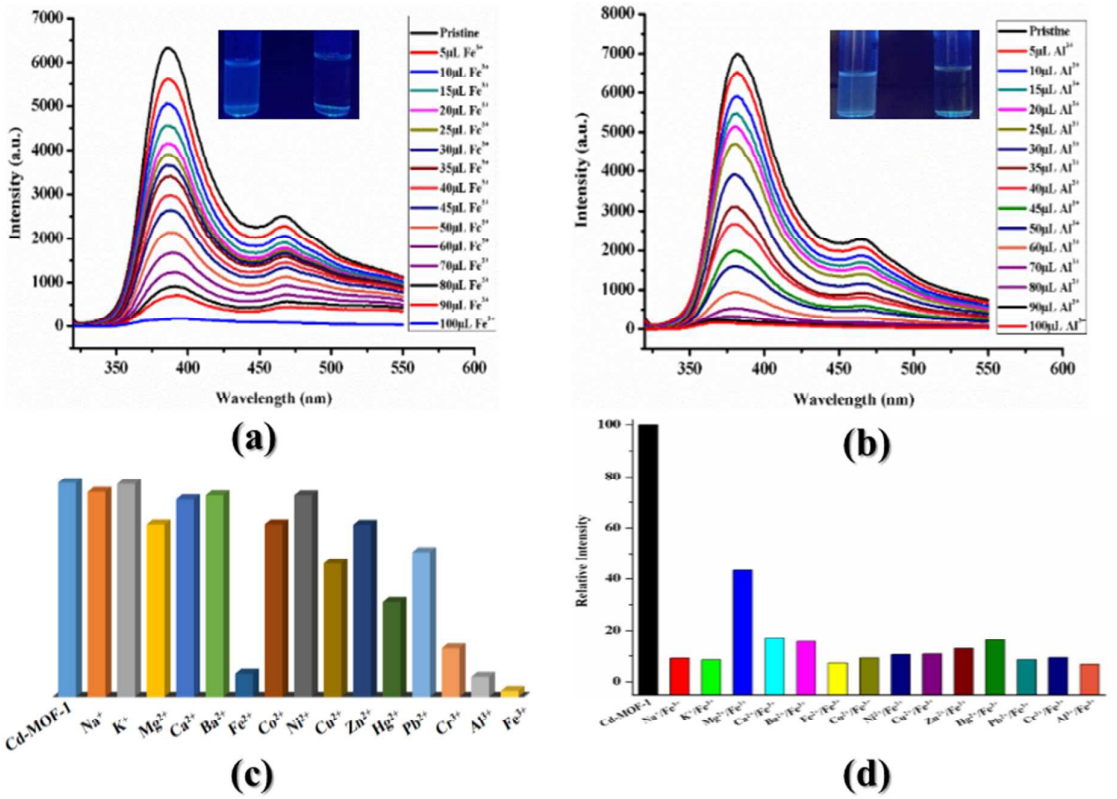

Fig. 3 (a) Photoluminescence spectra with a gradual addition of 10^{-2} (M) aqueous Fe^{3+} solution in the DMF dispersed solution of **Cd-MOF-1**. [Insets: colour changes before (left) and after (right) the addition of 100 μL Fe^{3+} solution (exposed to 365 nm UV light)] (b) Photoluminescence spectra with a gradual addition of 10^{-2} (M) aqueous Al^{3+} solution in the DMF dispersed solution of **Cd-MOF-1**. [Insets: colour changes before (left) and after (right) the addition of 100 μL Al^{3+} solution (exposed to 365 nm UV light)] (c) Relative luminescence intensities after introducing various metal cations. (d) Comparison of the fluorescence intensity of **Cd-MOF-1** exposed to mixed metal ions.

View Article Online
DOI: 10.1039/C8NJ02338G

reported results (Table S6 and S7, ESI), indicating the potential of **Cd-MOF-1** to act as a sensor towards highly sensitive and selective detection of Fe^{3+} ions. The limit of detection (LOD) value was determined by employing the equation: LOD = 3σ/K, where σ denotes the standard deviation of the initial intensity of **Cd-MOF-1** without analytes and K represents the slope of the linear curve. The estimated LOD value of **Cd-MOF-1** for Fe^{3+} is 2.4×10^{-6} M and 9.3×10^{-5} M for Al^{3+}.

Generally speaking, many metal ions coexist in practical biological and environmental system. Thus the interferences of the other metal ions for Fe^{3+}/Al^{3+} sensing also needs to be examined. 2 mL of MOF suspension containing mixed Fe^{3+} (50 μL 1×10^{-2} M) and each of rest of the cations (50 μL 1×10^{-2} M) were prepared and fluorescence intensity was measured. As shown in Fig. 4d the quenching emission effect was retained in the presence of the other cations, indicating that the quenching effects for the mixture of metal ions are not mutually interfered.

On the other hand, the luminescence property recorded for **Cd-MOF-2** is shown in Fig. S15 (ESI). Most of the metal ions have a different degree of quenching effect on the luminescence intensity of **Cd-MOF-2**. For example, the intensity at 312 nm is about the same (almost no quenching effect) with the original intensity when K^{+}, and Ba^{2+} are involved. On contrary, Fe^{3+} and Al^{3+} ions lead to almost complete quenching of intensity of **Cd-MOF-2**. These results indicate that **Cd-MOF-2** can selectively sense Fe^{3+} as well as Al^{3+} ions through luminescence quenching. As depicted in Fig. 4, the emission intensity of **Cd-MOF-2** decreases with gradually increasing the concentration of Fe^{3+} and Al^{3+} (5 μL to 100 μL) as could be observed for **Cd-MOF-1**. Hence, estimated from the plot of luminescence intensity and the concentration of the metal ions, the experimental result shows the value of K_{sv} = 4.9 $\times 10^{3}$ M^{-1}, and 2.6 $\times 10^{3}$ M^{-1} for Fe^{3+} and Al^{3+} respectively, which is higher and comparable as well with some literature reports (Table S6 and S7, ESI), indicating the potential of **Cd-MOF-2** to act as a sensor towards highly sensitive and selective detection of both of these ions. The quenching coefficient value K_{sv} for Fe^{3+} of **Cd-MOF-1** is roughly one order higher magnitude than that of **Cd-MOF-2**, which is probably because of the presence of azo functional groups lined open channels running along *a* axis in **Cd-MOF-1** compared to the dense framework of **Cd-MOF-2**. A similar trend is also observed for the case of Al^{3+}. The estimated LOD value of **Cd-MOF-2** for Fe^{3+} is 7.4×10^{-5} M and 6.1×10^{-5} M for Al^{3+}.

View Article Online
DOI: 10.1039/C8NJ02338G

As shown via the PXRD analysis, the skeleton of both the materials **Cd-MOF-1** and **Cd-MOF-2** remains unflawed, which contradicts the collapse of the network during quenching experiments. We speculate that the strong interaction between the Fe^{3+}/Al^{3+} ions and free Lewis basic azo sites of the frameworks is the possible reason for such luminescence quenching behavior. Moreover, the fluorescence response with respect to time was also recorded. As shown in Fig. S18 and S19 the fluorescence intensity of the MOF suspension with 10 µL of Al^{3+}/Fe^{3+} were continuously monitored after a certain period of time. There are no degree of enhancement or quenching effect with increasing the time. Hence the rapid response time may be attributed that both the metal ions Al^{3+} and Fe^{3+} can easily scatter into the channel of **Cd-**

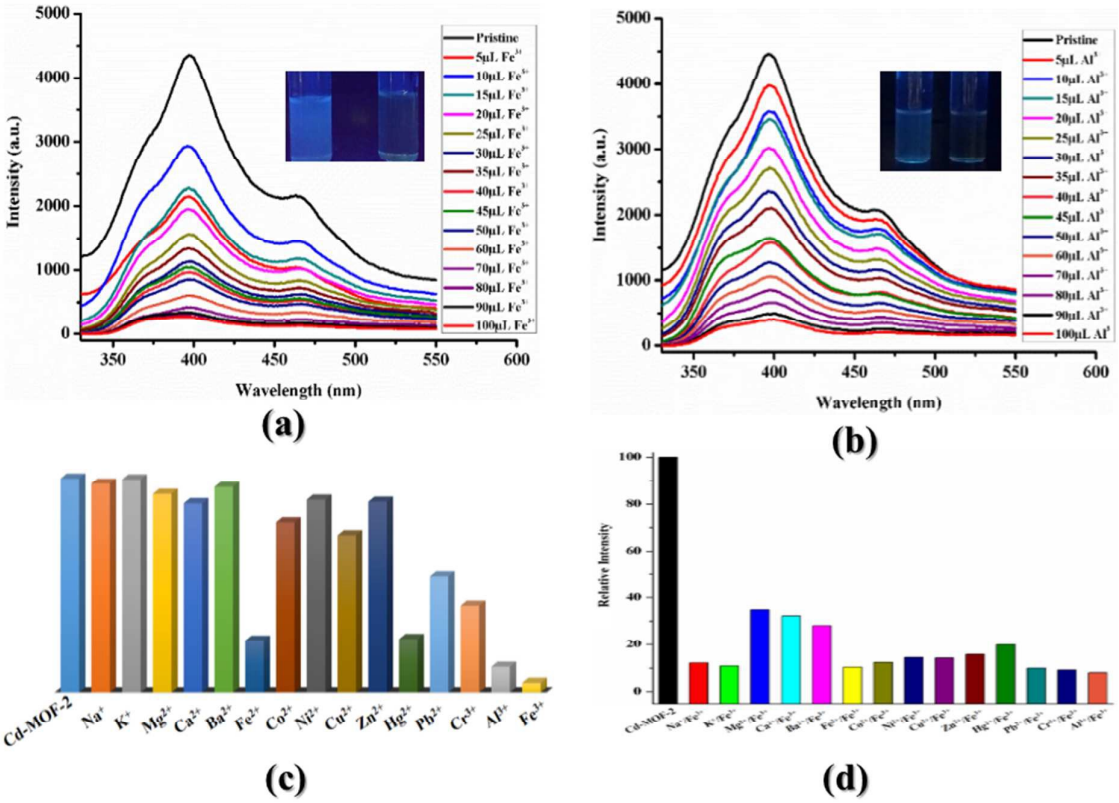

Fig. 4 (a) Photoluminescence spectra with a gradual addition of 10^{-2} (M) aqueous Fe^{3+} solution in the DMF dispersed solution of **Cd-MOF-2**. [Insets: colour changes before (left) and after (right) the addition of 100 µL Fe^{3+} solution (exposed to 365 nm UV light)] (b) Photoluminescence spectra with a gradual addition of 10^{-2} (M) aqueous Al^{3+} solution in the DMF dispersed solution of **Cd-MOF-2**. [Insets: colour changes before (left) and after (right) the addition of 100 µL Al^{3+} solution (exposed to 365 nm UV light)] (c) Relative luminescence

View Article Online
DOI: 10.1039/C8NJ02338G

intensities after introducing various metal cations. (d) Comparison of the fluorescence intensity of **Cd-MOF-2** exposed to mixed metal ions.

MOF-1 or may interact with the azo sites of the MOFs surfaces. The rapid response time is also higher than that of some previously reported materials.[15] It should be noted that the response time is rarely explored for the reported MOF-based ion sensors.

The possible mechanism for the sensing of Fe^{3+} ion would be explained by the followings: firstly, PXRD patterns of both the MOFs after the detection of Fe^{3+} ion were measured, which remained identical with their as-synthesized patterns suggesting that the skeleton of the MOFs remained intact under the experimental conditions (Fig. S5-S6, ESI). Hence, the quenching effect does not result from the destruction of the frameworks. To get a better insight into the phenomenon, the energy dispersive spectroscopy (EDS) elemental mapping of Fe^{3+} and Al^{3+}-loaded samples were performed. As shown in Fig. S24 to S27 (ESI), Fe and Al in both the samples are homogeneously distributed. Secondly, the resonance energy transfer is another possible reason for the quenching appearance of the framework due to sensing of the metal ions. The resonance energy transfer can be distinguished from the fluorophore (donor site) to the analyte (acceptor site), if the emission spectrum of the donor has a certain degree of overlap with the absorption spectrum of the acceptor, provided the appropriate distance between the donor and acceptor.[16] Hence, the UV-Vis spectra of the various metal ions in water has been investigated. It is observed from Fig. S28 and S29 (ESI) that there exists a large overlap between the absorption spectra of the Fe^{3+} ions and the emission spectra of both the **Cd-MOF**s whereas the other metal salts have no apparent overlap with the emission spectrum of the materials. For the Al^{3+} sensing, the quenching mechanism is not like Fe^{3+} as there is no existence of overlap between the absorption spectra of the Al^{3+} ions and the emission spectra of both the **Cd-MOF**s. The PXRD patterns of both the MOFs after the detection of Al^{3+} ion were measured, which shows the identical peak position with that of their as-synthesized patterns suggesting that the skeleton of the MOFs remained intact under the experimental conditions. The introduction of Al^{3+} metal ion may consume the energy through the collision interaction and further decrease the energy transfer from the spacer **L** to Cd^{2+} center may raise to the luminescence quenching.[17]

Conclusions

View Article Online
DOI: 10.1039/C8NJ02338G

In summary, two new 3D Cd-MOF based on an azo linked N,N′ donor spacer with two different dicarboxylates have been synthesized and structurally characterized. The luminescence investigation on both the materials manifested that both MOFs could act as dual luminescence sensors which can selectively and sensitively detect Al^{3+} as well as Fe^{3+} with rapid response time. The current result demonstrates the strategy of constructing luminescent MOFs through incorporation of functional bare azo sites onto the framework backbone for selective sensing of metal ions. Given that d^{10} transition metals are highly abundant and rich library of conjugated organic linkers and spacers for functional MOFs construction, this work may contribute to extend the potential application of transition metal based-MOFs toward dual-responsive luminescent probe for metal ion sensing.

Electronic Supplementary Information (ESI)

Crystallographic data, PXRD, TGA patterns, additional Figures related to sensing experiments, FESEM images, and EDS analysis study (PDF).

CCDC No: 1835623 for **Cd-MOF-1** and 1835624 for **Cd-MOF-2**

ORCID[iD]

Madhab C. Das: 0000-0002-6571-8705

Acknowledgments

S.C. thanks IIT KGP for SRF fellowship. M.C.D. gratefully acknowledges the financial support received from SERB, New Delhi as Early Carrier Research Award (ECR/2015/000041).

Notes and References

[1] J. D. Haas and T. Brownlie IV, *J. Nutr*., 2001, **131**, 676S−690S.

[2] L. Hyman and K. Franz, *Coord*. *Chem*. *Rev*., 2012, **256**, 2333−2356.

[3] (a) J. Barceló and C. Poschenrieder, *Environ*. *Exp*. *Bot*., 2002, **48**, 75-92.

[4] (a) B. Valeur and I. Leray, *Coord*. *Chem*. *Rev*., 2000, **205**, 3-40; (b) G. Berthon, *Coord*. *Chem*. *Rev*., 2002, **228**, 319-341.

[5] (a) L. E. Kreno, K. Leong, O. K. Farha, M. Allendorf, R. P. Van Duyne and J. T. Hupp, *Chem*. *Rev*., 2012, **112**, 1105−1125; (b) Y. Cui, Y. Yue, G. Qian and B. Chen,

View Article Online
DOI: 10.1039/C8NJ02338G

Chem. *Rev*., 2012, **112**, 1126−1162; (c) M. D. Allendorf, C. A. Bauer, R. K. Bhakta and R. J. T. Houk, *Chem*. *Soc*. *Rev*., 2009, **38**, 1330−1352; (d) W. P. Lustig, S. Mukherjee, N. D. Rudd, A. V. Desai, J. Li and S. K. Ghosh, *Chem*. *Soc*. *Rev*., 2017, **46**, 3242-3285; (e) T. K. Ghosh, S. Chakraborty, B. Chowdhury and P. Ghosh, *Inorg*. *Chem*., 2017, **56**, 5371− 5382; (f) B. Gole, A. K. Bar and P. S. Mukherjee, *Chem Commun*., 2011, **47**, 12137-12139; (g) S. Sanda, S. Parshamoni, S. Biswasa and S. Konar, *Chem*. *Commun*., 2015, **51**, 6576-6579; (h) M.-L. Gao, W.-J. Wang, L. Liu, Z.-B Han, N. Wei, X.-M. Cao and D. Yuan, *Inorg. Chem.* 2017, **56**, 511-517.

[6] (a) Y. Zhang, S. Yuan, G. Day, X. Wang, X. Yang and H.-C. Zhou, *Coord*. *Chem*. *Rev*., 2017, **354**, 28-45; (b) K. J. Waldron, J. C. Rutherford, D. Ford and N. J. Robinson, *Nature*, 2009, **460**, 823−830; (c) O. Braha, L. Q. Gu, L. Zhou, X. F. Lu, S. Cheley, and H. Bayley, *Nat*. *Biotechnol*. 2000, **18**, 1005−1007; (d) K. Jayaramulu, R. P. Narayanan, S. J. George and T. K. Maji, *Inorg*. *Chem*., 2012, **51**, 10089–10091; (e) K. S. Asha, R. Bhattachrjee and S. K. Mandal, *Angew Chem*. *Int*. *Ed*., 2016, **55**, 11528-11532; (f) G. Chakraborty and S. K. Mandal, *Inorg*. *Chem*., 2017, **56**, 14556–14566; (g) S. Pal and P. K. Bharadwaj, *Cryst*. *Growth Des*., 2016, **16**, 5852−5858; (h) L.-Y. Du, H. Wang, G. Liu, D. Xie, F.-S. Guo, L. Hou and Y.-Y. Wang, *Dalton Trans*., 2015, **44**, 1110–1119.

[7] (a) S. S. Nagarkar, B. Joarder, A. K. Chaudhari, S. Mukherjee and S. K. Ghosh, *Angew*. *Chem*., *Int*. *Ed*., 2013, **52**, 2881−2885; (b) Z. C. Hu, B. J. Deibert and J. Li, *Chem*. *Soc*. *Rev*., 2014, **43**, 5815−5840; (c) S. S. Dhankhar, N. Sharma, S. Kumar, T. J. D. Kumar, and C. M. Nagaraja, *Chem. Eur. J*., 2017, **23**, 16204 –16212; (d) G.-P. Li, G. Liu, Y.-Z. Li, L. Hou, Y.-Y. Wang, and Z. Zhu, *Inorg*. *Chem*. 2016, **55**, 3952−3959; (e) X.-D. Zhang, Y. Zhao, K. Chen, P. Wang, Y.-S. Kang, H. Wu and W.-Y. Sun, *Dalton Trans.*, 2018, **47**, 3958–3964; (f) Z.-Q. Liu, Y. Zhao, X.-D. Zhang, Y.-S. Kang, Q.-Y. Lu, M. Azam, S. I Al-Resayes and W.-Y. Sun, *Dalton Trans.,* 2017, **46**, 13943–13951.

[8] (a) B. Chen, L. Wang, Y. Xiao, F. R. Fronczek, M. Xue, Y. Cui and G. Qian, *Angew*. *Chem*. *Int*. *Ed*., 2009, **48**, 500−503; (b) J. Zhao, Y. N. Wang, W. W. Dong, Y. P. Wu, D. S. Li and Q. C. Zhang, *Inorg*. *Chem*., 2016, **55**, 3265−3271; (c) W. Yan, C. Zhang, S. Chen, L. Han and H. Zheng, *ACS Appl*. *Mater*. *Interfaces*, 2017, **9**, 1629−1634.

[9] (a) B. Wang, X.-L. Lv, D. Feng, L.-H. Xie, J. Zhang, M. Li, Y. Xie, J. Li and H.-C. Zhou, *J*. *Am*. *Chem*. *Soc*., 2016, **138**, 6204−6216; (b) B. Wang, Q. Yang, C. Guo, Y. Sun, L.-H. Xie and J.-R. Li, *ACS Appl*. *Mater*. *Interfaces*, 2017, **9**, 10286−10295; (c)

View Article Online
DOI: 10.1039/C8NJ02338G

C. X. Bezuidenhout, V. J. Smith, C. Esterhuysen and L. J. Barbour, *J. Am. Chem. Soc.* 2017, **139**, 5923-5929; (d) D. Zhao, X.-H. Liu, Y. Zhao, P. Wang, Y. Liu, M. Azam, S. I. Al-Resayes, Y. Lu and W.-Y. Sun, *J. Mater. Chem. A*, 2017, **5**, 15797–15807.

[10] (a) Z. Xiang, C. Fang, S. Leng and D. Cao, *J. Mater. Chem. A*, 2014, **2**, 7662–7665; (b) X.-Y. Dong, R. Wang, J.-Z. Wang, S.-Q. Zang and T. C. W. Mak, *J. Mater. Chem. A*, 2015, **3**, 641–647; (c) K. L. Wong, G. L. Law, Y. Y. Yang, W. T. Wong, *Adv. Mater.*, 2006, **18**, 1051–1054; (d) G. Ji, J. Liu, X. Gao, W. Sun, J. Z. Wang, S. Zhaoa and Z. L. Liu, *J. Mater. Chem. A*, 2017, **5**, 10200–10205.

[11] (a) R. Lv, H. Li, J. Su, X. Fu, B. Yang, W. Gu and X. Liu, *Inorg. Chem.*, 2017, **56**, 12348-12356; (b) L.-J. Han, W. Yan, S.-G. Chen, Z.-Z. Shi and H.-G. Zheng, *Inorg. Chem.*, 2017, **56**, 2936-2940; (c) Y.-J. Yang, M.-J. Wang and K.-L. Zhang, *J. Mater. Chem. C*, 2016, **4**, 11404-11418; (d) D. K. Singha and P. Mahata, *Inorg. Chem.*, 2015, **54**, 6373-6379.

[12] (a) S. Thies, H. Sell, C. Schutt, C. Bornholdt, C. Nather, F. Tuczek and R. Herges, *J. Am. Chem. Soc.*, 2011, **133**, 16243–16250; (b) C. B. Aakeroy, S. Panikkattu, B. DeHaven and J. Desper, *CrystEngComm*, 2013, ***15***, 463–470; (c) S. Chand, A. Pal and M. C. Das, *Chem. Eur. J.*, 2018, **24**, 5982-5986; (d) S. Chand, A. Pal, S. C. Pal, M. C. Das, *Eur. J. Inorg. Chem.* DOI: 10.1002/ejic.201800336.

[13] W.-M. Chen, X.-L. Meng, G.-L. Zhuang, Z. Wang, M. Kurmoo, Q.-Q. Zhao, X.-P. Wang, B. Shan, C.-H. Tunga and D. Sun, *J. Mater. Chem. A*, 2017, **5**, 13079–13085.

[14] Y. Salinas, R. Martinez-Manez, M. D. Marcos, F. Sancenon, A. M. Costero, M. Parra and S. Gil, *Chem. Soc. Rev.*, 2012, **41**, 1261−1296.

[15] (a) G.-G. Hou, Y. Liu, Q.-K. Liu, J.-P. Ma and Y.-B. Dong, *Chem. Commun.*, 2011, **47**, 10731–10733; (b) S. Dang, E. Ma, Z.-M. Sun and H. Zhang, *J. Mater. Chem.*, 2012, **22**, 16920-16926; (c) M. Zheng, H. Tan, Z. Xie, L. Zhang, X. Jing and Z. Sun, *ACS Appl. Mater. Interfaces*, 2013, **5**, 1078−1083.

[16] (a) S. R. Zhang, D. Y. Du, J. S. Qin, S. J. Bao, S. L. Li, W. W. He, Y. Q. Lan, P. Shen and Z. M. Su, *Chem. Eur. J.*, 2014, **20**, 3589−3594; (b) B.-L. Hou, D. Tian, J. Liu, L.-Z. Dong, S.-L. Li, D.-S. Li and Y.-Q. Lan, *Inorg. Chem.*, 2016, **55**, 10580−10586.

[17] (a) H. Xu, B. Zhai, C.-S. Cao and B. Zhao, *Inorg. Chem.*, 2016, **55**, 9671−9676; (b) H. Xu, M. Fang, C.-S. Cao, W.-Z. Qiao and B. Zhao, *Inorg. Chem.*, 2016, **55**, 4790−4794.

View Article Online
DOI: 10.1039/C8NJ02338G

Table of Content

Two Azo-functionalized Luminescent 3D Cd(II)-MOFs for Highly Selective Detection of Fe^{3+} and Al^{3+}

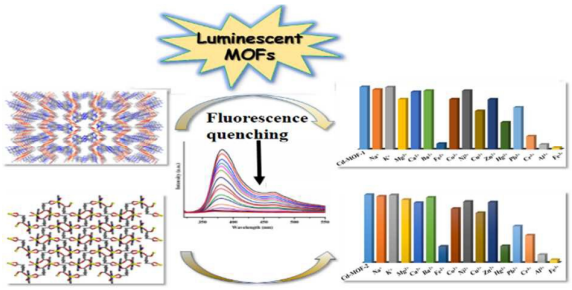

Two 3D luminescent Cd(II)-MOFs (**Cd-MOF-1** and **Cd-MOF-2**) exposing azo functional sites displayed selective detection of Fe^{3+} and Al^{3+} metal ions with high sensitivity.